Comments on Inorganic Chemistry
Publication details, including instructions for authors and subscription information:
http://www.informaworld.com/smpp/title~content=t713455155

RECENT ADVANCES IN THE STUDY OF MESOPOROUS METAL-ORGANIC FRAMEWORKS

Qian-Rong Fang[a]; Trevor A. Makal[a]; Mark D. Young[a]; Hong-Cai Zhou[a]
[a] Department of Chemistry, Texas A&M University, College Station, TX, USA

Online publication date: 02 December 2010

To cite this Article Fang, Qian-Rong , Makal, Trevor A. , Young, Mark D. and Zhou, Hong-Cai(2010) 'RECENT ADVANCES IN THE STUDY OF MESOPOROUS METAL-ORGANIC FRAMEWORKS', Comments on Inorganic Chemistry, 31: 5, 165 — 195
To link to this Article: DOI: 10.1080/02603594.2010.520254
URL: http://dx.doi.org/10.1080/02603594.2010.520254

Comments on Inorganic Chemistry, 31: 165–195, 2010

ISSN: 0260-3594 print
DOI: 10.1080/02603594.2010.520254

Taylor & Francis
Taylor & Francis Group

RECENT ADVANCES IN THE STUDY OF MESOPOROUS METAL-ORGANIC FRAMEWORKS

QIAN-RONG FANG, TREVOR A. MAKAL, MARK D. YOUNG, and HONG-CAI ZHOU

Department of Chemistry, Texas A&M University, College Station, TX, USA

Metal–organic frameworks (MOFs), which consist of metal ions or clusters and organic bridging ligands, have recently emerged as an important family of porous materials. In this comment, we discuss the current state of the field pertaining to MOFs with pore sizes between 2 and 50 nm, which have great application potential in gas storage, separation, sensor, catalysis, and drug delivery. This review will cover mesoporous MOFs containing 3-D channels, 1-D channels, and large cavities, as well as those based on supramolecular templates.

1. INTRODUCTION

Over the past half century, many porous materials have been discovered. These materials, both naturally occurring and man-made, have been investigated for potential applications that arise from their openings comparable to the sizes of various molecules.

Based on the difference of their composition, these porous materials can be classified into two types: inorganic and carbon-based materials.[1–5] For inorganic solids, the largest two subclasses are the aluminosilicate and aluminophosphate zeolitic materials, which are built from corner-sharing TO_4 tetrahedra (T = Al, Si, or P) that define

Address correspondence to Hong-Cai Zhou, Department of Chemistry, Texas A&M University, College Station, TX 77843. E-mail: zhou@chem.tamu.edu

interconnected tunnels or cages in which water molecules and metal ions are inserted.[1] Carbon-based porous materials, on the other hand, can be classified into two sub-categories: activated carbons, which are less defined structurally, as well as carbon nanotubes, nanofibers, nanohorns, and graphitic materials.

Adsorption of guest molecules onto the internal pore surface plays an important role in determining the properties and application potential of porous materials. The types of adsorption are defined not only by the interaction between guest molecules and the surfaces but also by the size and shape of the pores. Porous materials have been classified by the IUPAC based on their pore sizes: less than 2 nm as microporous, from 2 nm to 50 nm as mesoporous, and greater than 50 nm as macroporous.[6] As shown in Figure 1, there are six types of representative adsorption isotherms that reflect the relationship between porous structures and their sorption type.[7,8] These adsorption isotherms are characteristics of adsorbents that are microporous (Type I), nonporous (Types II and III), mesoporous (Types IV and V), and macroporous. Of these, Type IV isotherm is typical and given by many industrial mesoporous adsorbents. The most characteristic feature of a Type IV isotherm is the hysteresis loop, which is associated with capillary condensation taking place in mesopores.

As a new class of porous materials, metal–organic frameworks (MOFs, sometimes referred to as porous coordination polymers, PCPs)

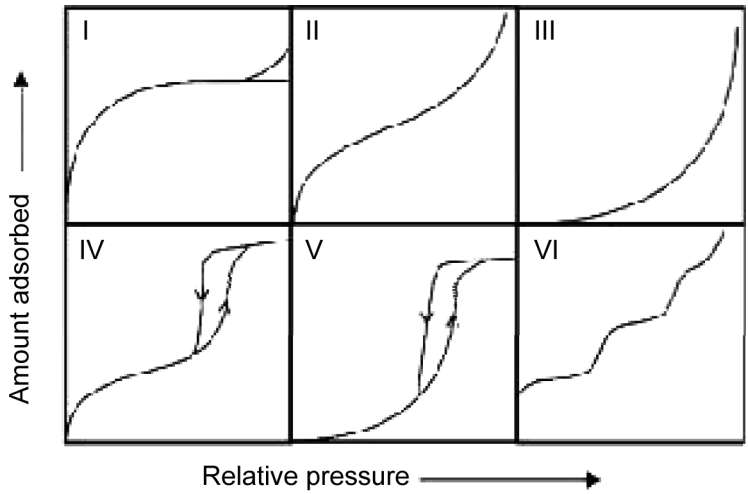

Figure 1. IUPAC classification of adsorption isotherms.

have undergone a rapid growth. MOFs represent a type of the inorganic-organic hybrid materials that bridge the two classes of porous materials (inorganic and carbon-based materials) discussed previously.[9–27] They are constructed from metal ions or metal ion clusters connected by organic linkers possessing carboxylates, phosphonates, or N-containing functional groups. Almost all elements of the periodic table, from alkaline earth metals to *p*-block elements, from transition metals to lanthanides and actinides, can be utilized in MOF construction.

The structural description and design of MOFs have been greatly facilitated by the use of the concept of secondary building units (SBUs).[14,16] Common SBUs are organic linkers, which are normally not discussed, and the inorganic clusters (discrete or infinite). The linking of these SBUs in a periodic fashion results in the creation of a MOF (Figure 2). A topological approach may also be utilized to simplify structural description and design.[28–30]

The development of MOFs has attained a mature level in a surprisingly short period of time. As a new type of porous materials, MOFs can exhibit from micro- to meso-sized cavities and/or open channels, which are arranged regularly in a crystal lattice. Their syntheses occur under

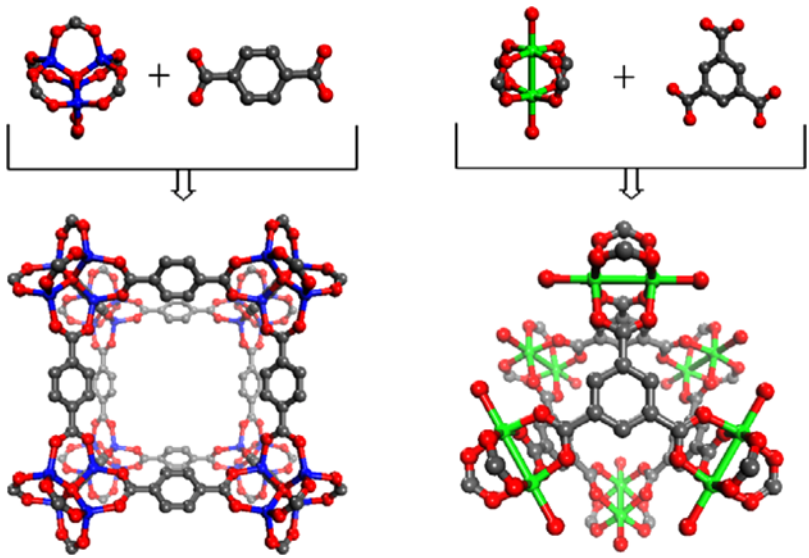

Figure 2. Illustration of MOF synthesis and chemical composition: MOF-5[24] (left) and HKUST-1[27] (right). (Figure appears in color online.)

mild conditions and to some extent, their structure and porosity can be designed based on SBUs. MOFs possess advantages of both organic and inorganic materials including open coordination sites and functional groups.[31] The surface area of a MOF can reach many times of those of other porous materials and the property of the internal surface is tunable, giving rise to a great number of potential applications, such as gas separations and storage, catalysis, as well as drug delivery. New functional materials based on postsynthetic modification can also be obtained.[32–37]

In order to expand the utility of MOFs in areas such as macromolecular catalysis and separation, MOFs with pores larger than 2 nm have captivated chemists and material scientists who are interested in studying chemistry and physics in a confined space. A number of these mesoporous MOFs have been recently reported (Table 1).[38–49] The concept of a mesoporous MOF is not new, sharing the same relationship as other mesoporous materials, with the size of the pores ranging from 2 nm to 50 nm. However, because crystal structures of MOFs are more accessible than other porous materials, the pictures of the internal pores are clearer than ever before. Presently, the pores of mesoporous MOFs refer not only to channels but also cavities. MOF materials with large cavities (>20 Å) but small connecting channels (<20 Å), such as MIL-100 and MIL-101, are also described as mesoporous MOFs, even though they do not exhibit the Type IV isotherm.[42,43] Additionally, the potential advantages offered by mesoporous MOFs can be appreciated by the following considerations: (1) as mentioned in the foregoing discussion, unlike traditional mesoporous materials, mesoporous MOFs are completely ordered crystalline materials whose structures can usually be solved by single-crystal X-ray diffraction; (2) the structure and porosity of the mesoporous MOFs are tunable. The desired extended network can be easily obtained by the choice of organic linkers, metal cluster SBUs, and post-synthetic modifications; (3) these mesoporous MOFs may have very large surface areas ($\sim 6000\ m^2/g$), which will give rise to a number of potential applications in gas storage and separation, although new models need to be developed to calculate the effective surface area of a mesoporous MOF.

This comment starts with a brief survey of the progress and applications in traditional mesoporous materials. The remainder of the comment will focus on mesoporous MOFs, which are organized by pore shapes and structures of the materials including mesoporous MOFs with

Table 1. The characterization of mesoporous MOFs

Compounds	Windows or channels (nm)	Cavities (nm)	Surface Area/m^2g^{-1} BET	Surface Area/m^2g^{-1} Langmuir	Pore vol./cm^3	Type of N_2 adsorption isotherm	Ref.
IRMOF-16	2.9						38
MesoMOF-1	2.2 × 2.61					Type IV	39
JUC-48	2.5 × 2.8			880		Type I	40
UMCM-1	2.4 × 2.9	1.4 × 1.7		6500		Type I with secondary uptakes	41
MIL-100	1.2	2.5 × 2.9		3100	1.16	Type I	42
MIL-101	1.4 × 1.6	2.9 × 3.4	4100	5900	2.0	Type I with secondary uptakes	43
MIL-101_NDC	1.35 and 1.82 × 2.03	3.9 and 4.6	2100			Type I with secondary uptakes	44
$Tb_{16}(TATB)_{16}(DMA)_{24}$	1.3 and 1.7	3.9 and 4.7	1783	3855		Type I with third uptakes	45
UMCM-2		2.6 × 3.2	5200	6060		Type I with secondary uptakes	46
ZIF-95	0.37	2.5 × 1.4 and 3.0 × 2.0	1050	1240		Type I	47
ZIF-100	0.35	3.56	595	780		Type I	47
$Cu_3(btc)_2(H_2O)_3$	3.8 to 31.0		533 ~ 1225			Type IV	48
PCN-61		2.3, 1.5, and 1.3	3000	3500	1.36	Type I with secondary uptakes	49
PCN-66		2.6, 1.6, and 1.3	4000	4600	1.63	Type I with secondary uptakes	49

3-D channels, 1-D channels, and large cavities. Mesoporous ZIFs (zeolitic imidazolate frameworks, a subclass of MOFs) with large cavities will be studied. In addition, mesoporous MOFs based on supramolecular templates are also presented. Sequentially, the applications of mesoporous MOFs are discussed; these include gas storage/separation, sensor, catalysis, and drug delivery. A short summary and a few remarks on future directions will conclude the comment.

2. TRADITIONAL MESOPOROUS MATERIALS

Traditional mesoporous materials include mesoporous silica and alumina. Mesoporous oxides of niobium, tantalum, titanium, zirconium, cerium, and tin have also been reported.[4,50–55] At present, more than 20 common mesoporous materials are available differing in channel size, channel connectivity, chemical composition, and structure directing agents applied during synthesis. Although the term mesoporous defines materials with pores in the range 2–50 nm, the most common usage implies that such materials with uniform pores are often ordered to produce a distinct X-ray diffraction pattern. These patterns usually consist of only several diffraction lines located at low angles owing to the absence of crystalline phases but long-range ordering. A direct approach to mesoporous materials with organic functional groups involves so-called periodic mesoporous organosilicas.[56] These materials are prepared from substituted orthosilicates, optionally in the presence of tetraethyl orthosilicate (TEOS) or analogous hydrolyzable moieties.

Long range ordering was first achieved for a mesoporous material in 1990.[57] Around that time, the synthesis was also conducted by the group of the former Mobil Oil Company.[4,50] Since then, research in this field has steadily grown. The original work from Mobil referred to the new materials as M41S family and identified three basic silicate-based structures akin to surfactant lyotropic liquid crystal phases, namely hexagonal, cubic, and lamellar with the corresponding designation MCM-41, MCM-48, and MCM-50.[4] The M41S materials were obtained under conditions similar to zeolite synthesis but with cationic surfactants. MCM-41 consisted of 1-D parallel channels with pores up to 10 nm and large internal pore area exceeding 1000 m^2/g. The ease of preparation made MCM-41 the most widely studied mesoporous material up to now. MCM-48 contains a 3-D channel system, which made it more attractive than MCM-41. However, it was more difficult

to synthesize, and only after some convenient preparation routes were identified the catalytic applications of MCM-48 were more systematically pursued. In addition, the use of different surfactants afforded many new structures expanding the dimensions and nature of the available pore systems. With regard to catalytic application the one-dimensional hexagonal and cubic structures have been the primary focus, such as SBA-15 obtained with block co-polymers and MSU-type with neutral amine templates.[58,59]

Although not all of the original expectations of these materials were fulfilled, particularly due to the lack of strong Brønsted acid sites and lower (hydro)thermal stability when compared with zeolites, mesoporous materials are interesting ordered materials with a high potential in adsorption, drug delivery, gas sensing, optics, photovoltaics, and particularly in catalysis.[4,50] Aluminosilicate versions of the mesoporous materials were studied and developed first showing significant activity in catalytic conversions of hydrocarbons.[60] The large pores and surface areas combined with amorphous walls containing many hydroxyl groups allowed for additional functionalization and a vastly expanding potential for generating catalytic materials. For instance, mercaptopropylsiloxanes on MCM-41 can be easily oxidized to sulfonic groups and serve as highly active acid catalysts for transesterification.[61,62]

3. THE CLASSIFICATION OF MESOPOROUS MOFs

Compared with microporous MOFs, it is only the beginning for the preparation of those MOF materials with mesopores, which still remain largely unexplored. Since Yaghi *et al.* for the first time reported a mesoporous MOF, IRMOF-16, by utilizing the large organic ligand, TPDC (TPDC = [1,1′:4′,1″-terphenyl]-4,4″-dicarboxylic acid),[38] several other mesoporous MOFs have been recently prepared, including mesoporous MOFs with 3-D channels, 1-D channels and large cavities, mesoporous ZIFs with large cavities, as well as mesoporous MOFs based on supramolecular templates. While the IUPAC defines traditional mesoporous materials as being composed of pores within the range of 2 nm to 50 nm and possessing a type IV isotherm, it is worth noting that few mesoporous MOFs show a type IV isotherm (Table 1). The reason is that the adsorption profiles of mesoporous MOFs mainly depend on their unique pore shapes, which are governed by the size of the accessible window into the pore. So, while the Type I isotherm is usually indicative of a

traditional microporous material, this same type of isotherm but with second uptake is observed for MOF materials in which microporous windows open to mesoporous cages. As the size of the windows increase towards 2 nm, creating a mesoporous channel, the expected Type IV isotherms are measured (Figure 3).[39]

3.1. Mesoporous MOFs with 3-D Channels

The increase of the channel sizes of MOFs to mesoporous range (2–50 nm) is still a great challenge. Ligand extension is an apparent strategy, but open MOFs built from large ligands tend to disintegrate after the removal of guest molecules. Another difficulty in the preparation of a mesoporous MOF by ligand extension is that such MOFs are often accompanied by framework interpenetration that will drastically reduce the size of the pores. Therefore the construction of mesoporous MOFs should be guided by the extension of the ligand while inhibiting interpenetration and reinforcing the framework against collapse upon guest removal.

In 2002, Yaghi *et al.* prepared the first 3-D mesoporous MOF, IRMOF-16, by successfully using a long linker, TPDC.[38] This MOF has the expected topology of CaB_6 adapted by the prototype IRMOF-1 (also named as MOF-5) in which an oxide-centered Zn_4O tetrahedron is edge-bridged by six carboxylate groups to give the octahedron-shaped SBU that reticulates into a 3-D cubic porous network. In the structure of IRMOF-16, the free- and fixed-diameter values are 19.1 Å and 28.8 Å, respectively. The upper limit is in the mesoporous range (from

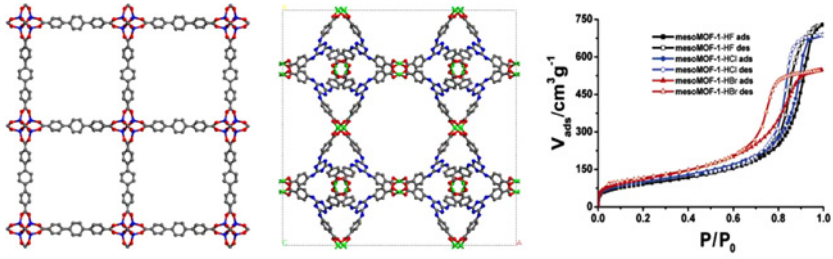

Figure 3. Structural representations of IRMOF-16 with cubic channels of 28.8 $Å^2$ (a) and mesoMOF-1 with open channels of 22.5×26.1 $Å^2$ (b) as well as N_2 sorption isotherms of mesoMOF-1-HX (c). (Reproduced with permission from Wang et al.[39] Copyright 2006: American Chemical Society.) (Figure appears in color online.)

2 nm to 50 nm). The percent free volume in crystal of IRMOF-16 is 91.1%, greatly exceeding the values found in some of the most open zeolites, such as faujasite,[63] in which the free space is 45 to 50% of the crystal volume. The calculated crystal density (in the absence of guests) of IRMOF-16 is as low as $0.21\ g/cm^3$. The density of IRMOF-16 is the lowest reported for any crystalline material known to date. Although no further characterization about N_2 adsorption was provided, it was believed to be likely that such reticular chemistry may be used more routinely toward the design and synthesis of crystalline and fully ordered mesoporous crystals.

Zhou and co-workers also reported a non-interpenetrated mesoporous MOF, mesoMOF-1, from a newly designed ligand TATAB (TATAB = 4,4′,4″-*s*-triazine-1,3,5-triyltri-*p*-aminobenzoate) containing hierarchical functional groups.[39] In this structure, two copper atoms are bridged by four carboxylate groups to form the well-known paddle-wheel SBU with axial aqua ligands. Each SBU connects four TATAB ligands, and each TATAB binds three SBUs to form a T_d octahedron, in which all six vertices are occupied by the SBUs, and four of the eight faces are spanned by TATAB ligands. Eight of these T_d octahedra occupy the eight vertices of a cube to form a cuboctahedron through corner sharing. The three-dimensional framework with twisted boracite net topology is then formed by the propagation of these cuboctahedra. Open channels from all three orthogonal directions are identical in size and are as large as $22.5 \times 26.1\ Å^2$ (atom to atom distances). To stabilize the meso-channels, acids (HX, X=F, Cl, Br) have been used to react with the amino groups in TATAB to afford ionic frameworks. The treatment with the acids leads to protonation of the amino groups in the TATAB ligand, and the protonated frameworks showed significantly higher thermal stability than the unmodified analogue as indicated by thermogravimetric analyses. Interestingly, nitrogen sorption measurements on the protonated samples revealed a typical Type IV behavior, indicating the mesoporous nature of these materials. It represents the first example exhibiting a Type IV adsorption-desorption isotherm in MOFs.

3.2. Mesoporous MOFs with 1-D Channels

Aside from extending organic ligands to obtain mesoporous MOFs, two other synthetic strategies have also been employed to build up porous MOFs with large 1-D channels: the construction of infinite rod-shaped

SBUs and the mixture of two different organic ligands. By constructing infinite rod-shaped SBUs, the framework of the compound will form an impenetrable wall, which prohibits additional ligands from filling in between adjacent linkers and the interpenetrated structure. Although experimental data are lacking for mixing two different linkers possessing the same coordinating functionality, this method represents an expeditious route to discover new porous solids, mesoporous materials in particular.

As an example of constructing infinite rod-shaped cadmium carboxylate SBUs, Qiu *et al.* described the synthesis and structure of a mesoporous MOF, JUC-48, from a rigid and linear organic O-donor ligand, bpdc (bpdc = 4,4′-biphenyldicarboxylate), as a linker.[40] In this MOF, Cd(II) centers are linked together by carboxylate groups of bpdc to construct 1-D Cd-O-C chains running along the [001] direction. These Cd-O-C chains, as rod-shaped SBUs, are interconnected through the biphenyl groups of bpdc to generate a 3-D non-interpenetrating extended network with 1-D hexagonal channels of 24.5×27.9 Å^2 viewed along the [001] direction. Each hexagonal channel of JUC-48 can be viewed as a nanotube-like architecture. Furthermore, by reducing the structure of JUC-48 to simple rod geometries and associated nets, the framework of JUC-48 is a threefold connected 3-D network with a rare etb topology. The permanent porosity of JUC-48 is confirmed by its N_2 adsorption isotherm, which is only a typical Type I behavior and reveals a Langmuir surface area of 880 m^2g^{-1} (Figure 4).

Subsequently, the Matzger group synthesized the other mesoporous compound with 1-D hexagonal channels, UMCM-1, based on two

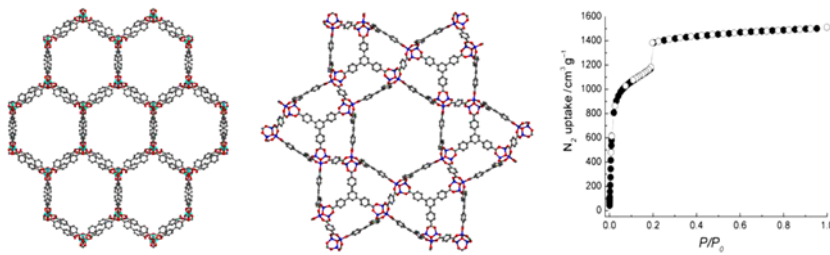

Figure 4. Structural representations of JUC-48 with 1-D hexagonal channels of 24.5×27.9 Å^2 (a) and UMCM-1 with 1-D hexagonal channel of 27×32 Å^2 (b) as well as N_2 sorption isotherm of UMCM-1 (c). (Reproduced with permission from Koh et al.[41] Copyright 2008: Wiley-VCH Verlag GmbH & Co. kGaA.) (Figure appears in color online.)

organic linkers with different topologies, terephthalic acid (H_2BDC) and 1,3,5-tris(4-carboxyphenyl)benzene (H_3BTB).[41] The framework of the material consists of Zn_4O clusters linked together by two BDC and four BTB linkers arranged in an octahedral geometry with the two BDC linkers adjacent from one another, leaving the other four positions occupied by BTB linkers. These octahedra assemble into a structure containing both microporous cages and mesoporous channels. The microporous cages are constructed from six BDC linkers, five BTB linkers, and nine Zn_4O clusters, with an internal dimension of approximately $14 \times 17\ \text{Å}^2$. The 1-D hexagonal mesoporous channels ($27 \times 32\ \text{Å}^2$) are assembled from the convergence of six such microporous cages in an edge-sharing fashion. The microporous nature of the framework is made apparent when considering the N_2 uptake of UMCM-1. The uptake up to the first plateau is $1200\ \text{cm}^3\ \text{g}^{-1}$, indicating a calculated Langmuir surface area of $4730\ \text{m}^2\ \text{g}^{-1}$. The second plateau provides a Langmuir surface area of $6500\ \text{m}^2\ \text{g}^{-1}$ ($>1400\ \text{cm}^3\ \text{g}^{-1}$ N_2 adsorption, Figure 4).

3.3. Mesoporous MOFs with Large Cavities

Mesoporous MOFs with large cages (i.e., a mesoporous cavity surrounded by microporous windows) are the most common materials in the family of mesoporous MOFs. A series of mesoporous MOFs with large cages has been prepared by changing organic linkers, utilizing rare-earth metal ions or mixing different ligands.[42–46] In some cases, the application of conventional small molecule chemical crystallographic methods has proven very difficult to achieve a structural solution of mesoporous MOFs. A new computational strategy to solve the crystal structures of mesoporous MOFs has been developed, utilized for the compounds MIL-100, MIL-101 and MIL-101_NDC.[42–44] Using computational simulation techniques, exploration may begin to identify how an inorganic cluster and an organic linker, or even predefined hybrid building blocks, may connect in 3-D space to form a periodic lattice.

In 2004, Férey *et al.* have shown from a straightforward example the strength of the combined chemistry–simulation approach for obtaining new materials (Figure 5). By the combination of Cr^{3+} ions with trimesic acid, BTC (BTC = benzene-1,3,5-tricarboxylate), under hydrothermal conditions, a new powdered chromium hybrid solid (MIL-100) was prepared.[42] The crystal structure of MIL-100 was obtained by using

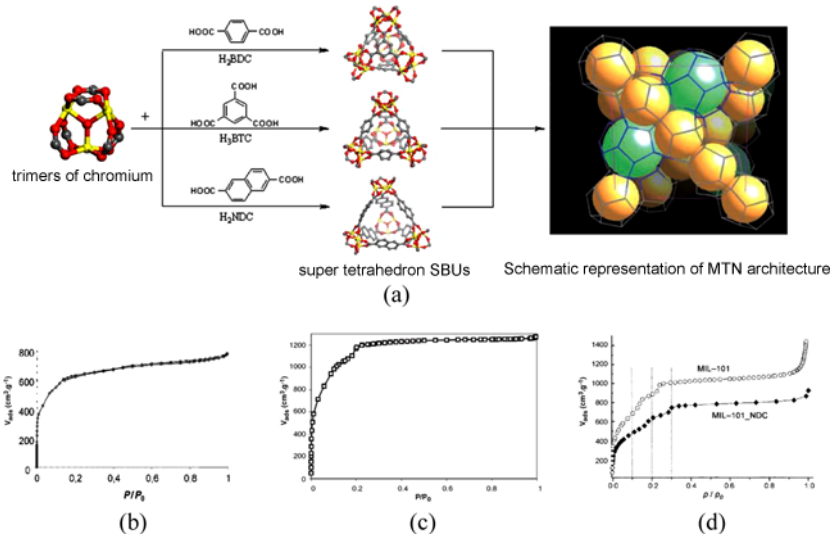

Figure 5. (a) Structural representations of MIL-100 with larger cavities of 29 Å (top), MIL-101 with larger cavities of 34 Å (middle) and MIL-101_NDC with accessible cages of 46 Å (bottom); (b), (c) and (d) N_2 sorption isotherm of MIL-100, MIL-101 and MIL-101_NDC, respectively. (Reproduced with permission from Ferey and Serre et al.[42] Copyright 2004: Wiley-VCH Verlag GmbH & Co. KGaA (a), Ferey and Mellot-Draznieks et al.[43] Copyright 2005: AAAS (b), and Sonnauer et al.[44] Copyright 2009: Wiley-VCH Verlag GmbH & Co. KGaA (c).) (Figure appears in color online.)

original global optimization simulations, which was based on the concept of SBUs to assemble organic and inorganic units. This is the first time, in the field of hybrid solids, that a rational simulation approach provides a solution of the crystal structure constructed only from topological criteria, which matches the experimental X-ray diffraction pattern of the solid. In its framework, BTC and inorganic trimers built up a large super tetrahedron (ST) with an internal diameter of 6.6 Å. Interestingly, the corner sharing of the ST delimits a framework with two types of cages, whose dimensions are typically in the range of mesopores. The smallest cage, made up from 20 ST, has an internal diameter of about 25 Å. The polyhedron obtained by joining the centers of the ST is a pentagon dodecahedron with free opening of 4.8×5.8 Å^2. The subnetwork that joins these centers forms corner-linked tetrahedra as in the pyrochlore structure. The dodecahedra share faces and form infinite linear rodlike chains, which cross orthogonally to each other through common

faces to ensure the 3-D network. This connection creates larger cavities, which have 28 ST. The polyhedron determined by the centers of the ST has now 12 pentagonal and 4 hexagonal faces. The aperture of the large hexagonal windows is about $8.6 \times 8.6\,\text{Å}^2$ and the internal diameter is approximately 29 Å. As stated by Férey, this compound provides the first example of a porous solid with crystalline walls and a unique hierarchical system of three types of cages of different dimensions. The thermal behavior and the sorption properties of MIL-100 were investigated. The thermal gravimetric analysis carried out in air reveals an interesting stability of MIL-100 up to 275°C. The gaseous N_2 sorption isotherm on the fully evacuated samples is Type I with a slight secondary uptake, which is indicative of the presence of both micro-and mesopores. By using the Dubinin-Raduskhvich equation, MIL-100 showed a pore volume of $1.16\,\text{cm}^3\,\text{g}^{-1}$. For a monolayer coverage of N_2, the apparent Langmuir surface area was estimated up to 3100(40) m^2g^{-1}.

The combination of targeted chemistry and computational design to create a crystal structure was further investigated by Férey and co-workers through using terephthalic acid [1,4-benzene dicarboxylate (1,4-BDC)] combined with similar trimers.[43] The resulting solid, MIL-101, has the best characteristics in terms of cell dimensions ($702{,}000\,\text{Å}^3$), pore sizes (29 to 34 Å), and surface area ($5900\,\text{m}^2\,\text{g}^{-1}$). In this compound, a ST was built from the linkage of 1,4-BDC anions and inorganic trimers that consist of three iron atoms in an octahedral environment with four oxygen atoms of the bidendate dicarboxylates, one μ_3O atom, and one oxygen atom from the terminal water or fluorine group. The iron octahedra are thus related through the bridging μ_3-O atom to form the trimeric building unit. The four vertices of the ST are occupied by these trimeric units, with the six edges hosting the organic linkers. The ST are connected through corner sharing, creating a three-dimensional network. The STs are microporous (with an 8.6 Å free aperture for the windows), and the resulting framework delimits two types of mesoporous cages filled with guest molecules. These two cages, which are present in a 2:1 ratio, are enclosed by 20 and 28 ST with internal free diameters of ~29 Å and 34 Å, respectively. These values correspond to accessible pore volumes of $\sim 12{,}700\,\text{Å}^3$ and $\sim 20{,}600\,\text{Å}^3$, respectively. The windows to these cages are ~12 Å for the smaller cage and ~14.5 Å and 16 Å for the larger cage. Thermogravimetric analysis in air revealed that MIL-101 was stable up to 275°C. The N_2 sorption isotherm on the dehydrated sample is of Type I with secondary

uptakes at $P/P_0 \sim 0.1$ and at $P/P_0 \sim 0.2$, characteristic of the presence of the two kinds of microporous windows. A pore volume near 2.0(1) $cm^3 g^{-1}$ for MIL-101 was obtained by using the Dubinin-Raduskhvich equation. The apparent Brunauer-Emmer-Teller (BET) and Langmuir surface area are measured to be 4,100(200) and 5,900(300) m^2g^{-1}, respectively.

Most recently, by employing a high-throughput reactor, Férey and Stock *et al.* reported the synthesis and characterization of the chromium 2,6-naphthalenedicarboxylate MIL-101_NDC, the structure model of which was constructed by means of molecular simulation techniques.[44] As with the structure of MIL-101, MIL-101_NDC is in close relationship to the augmented zeolite Mobil Thirty-Nine (MTN) structure type. The structure is based on ST, which consist of trimeric $[Cr_3(OH)(H_2O)_2(\mu_3\text{-}O)]$ units that are linked along the edges by the naphthalenedicarboxylate ions. The free aperture of the ST windows is about 10.2 Å. The framework is constructed of pentagonal (5 ST) and hexagonal rings (6 ST) that form two types of mesoporous cages. The smaller dodecahedral cage (5^{12}; 20 ST) consists only of pentagonal rings with a free diameter of approximately 13.5 Å, and the diameter of the accessible cavity is about 39 Å. The larger hexacaidecahedral cage ($5^{12}6^4$; 28 ST) incorporates pentagonal and hexagonal rings with a free aperture of the hexagonal windows of approximately 18.2×20.3 $Å^2$ and an accessible cage diameter of approximately 46 Å. The two types of cages are present in a small/large ratio of 2:1. Transmission electron microscopy (TEM) investigations of activated MIL-101_NDC showed the presence of thin (less than 100 nm) plates, consisting of a crystalline MIL-101_NDC core (average diameter ca. 100 nm) and an X-ray-amorphous shell (thickness ca. 25 nm). The porosity of MIL-101_NDC was investigated by nitrogen sorption experiments at 77 K. The isotherm is Type I, with pore-filling steps at $P/P_0 \approx 0.2$ and $P/P_0 \approx 0.3$, characteristic of the presence of two types of narrow mesopores. The surface area of $S_{BET} = 2100(100)$ $m^2 g^{-1}$ was measured for the activated sample. This small surface area can be explained by the presence of the X-ray amorphous shells surrounding the crystalline core.

From the above examples, it is not difficult to realize that the structural details of mesoporous MOFs with large cages are sacrificed as the pore size increases, and thus are likely to be solved by means of computational simulation techniques. However, Kim and co-workers report the crystal structure of a rare-earth mesoporous MOF with fused 3.9 and 4.7 nm cages (Figure 6), which can be directly determined at atomic

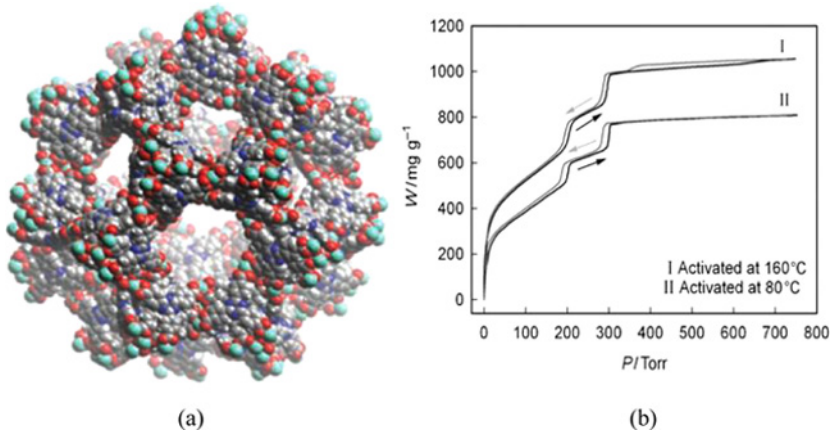

Figure 6. Representation of largest cavities with 47 Å (a) and N_2 sorption isotherm (b) of rare-earth mesoporous MOF. (Reproduced with permission from Park et al.[45] Copyright 2007: Wiley-VCH Verlag GmbH & Co. KGaA.) (Figure appears in color online.)

resolution by X-ray crystallography.[45] In its crystal structure, each Tb_4 unit has a trigonal-planar geometry with an average interatomic distance of 5.14 Å between the peripheral atoms and the central atom. The separation between two peripheral Tb^{3+} ions is about 8.82 Å. In turn, four Tb_4 moieties form a ST, with a separation of about 16.27 Å between the central Tb^{3+} ions. The unit cell is comprised of sixty-eight of these ST. There exist five and six-membered rings in the framework, which, considering van der Waals radii, have free diameters of 13.0 and 17.0 Å, respectively. These openings are windows into two large cages. The smaller cage, called "S" by Kim et al., is bound by 20 ST and has 12 pentagonal windows. Its internal free diameter is 39.1 Å. The larger cage "L" is bound by 28 STs with 12 pentagonal and 4 hexagonal windows. Its internal free diameter is 47.1 Å. A nitrogen adsorption measurement on the evacuated as-prepared crystals at 77 K and up to 760 Torr showed a nearly reversible isotherm with three uptakes. When the samples were activated at 160°C, the surface area values increased to 1783 m^2 g (BET) and 3855 m^2 g (Langmuir).

The Matzger group recently reported another example with large cages, UMCM-2 (Figure 7), that can also be directly determined at atomic resolution by X-ray crystallography.[46] A 1:1 mixture of two ligands, T^2DC (thieno[3,2-b]thiophene-2,5-dicarboxylate) and BTB, in conjunction with zinc ions was used to produce this framework.

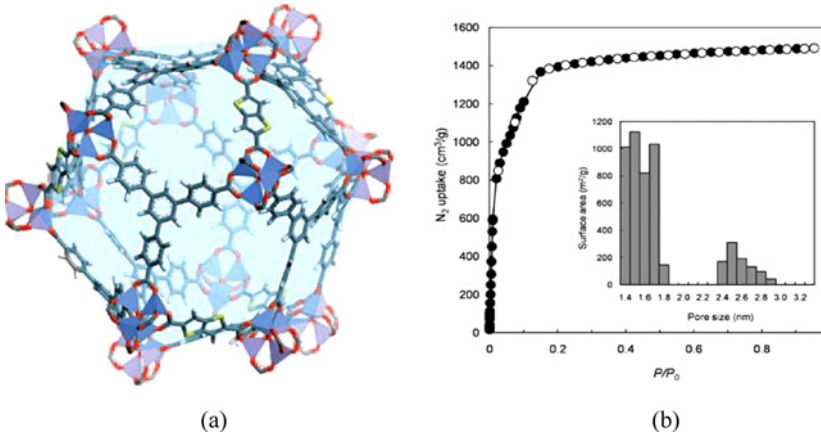

Figure 7. Representation of largest cavities with 32 Å (a) and N_2 sorption isotherm (b) of UMCM-2. (Reproduced with permission from Koh et al.[46] Copyright 2009: American Chemical Society.) (Figure appears in color online.)

UMCM-2 consists of Zn_4O metal clusters linked together by two T^2DC and four BTB ligands, forming two different microporous cages (denoted Cages I and III by the authors) and a mesoporous cage (Cage II). Cage I has the same geometry as the microporous cage of UMCM-1. Cage II has an internal van der Waals dimension of approximately 2.6 nm × 3.2 nm. The organization of Cages I and II forms the second microporous cage, Cage III. The nitrogen uptake of UMCM-2 was measured at ~1500 cm^3/g. Using the value at the first plateau ($P/Po \approx 0.1$), the BET and Langmuir surface areas were calculated to be 5200 m^2/g and 6060 m^2/g, respectively.

The Zhou group reported two additional MOFs with large cages, PCN-61 and PCN-66.[49] The isostructural MOFs based on the (3,24)-connected network are composed of dicopper paddlewheel SBUs and hexatopic organic linkers possessing C_3 symmetry, 5,5′,5″-benzene-1,3,5-triyltris(1-ethynyl-2-isophthalate) (btei) and 5,5′,5″-(4,4′,4″-nitrilotris(benzene-1,4-diyl)tris(ethyne-1,2-diyl)) triisophthalate (ntei), respectively. The designed organic linkers led to the formation of three different types of polyhedral cages in the framework including cuboctahedral, truncated tetrahedral and truncated octahedral cages. The cubocatahedral cages are formed from the isophthalate moieties binding the SBUs and are invariant upon lengthening of the organic linker. Therefore, the cuboctahedral cages are of similar size in both frameworks, and may

be inscribed by a sphere with diameter 13 Å. These microporous cages lead to a great increase in the stability of the overall frameworks, which may be modified by extending the length from the central point to the isopthalate moieties. Extending the distance from the central point of the linker to the isopthalate moieties permits an increase in the pore size and surface area of the isostructural framework with little other impact. Analysis of the limits of this extension is currently being investigated.

3.4. Mesoporous ZIFs with Large Cavities

Currently, Yaghi and others have been systematically exploring MOFs based on metal imidazolates that share many of the advantages of zeolite chemistry.[64–68] These compounds have been named zeolitic imidazolate frameworks (ZIFs) to highlight this relationship. ZIFs are porous crystalline materials with tetrahedral networks that resemble those of zeolites: transition metals (Zn, Co) replace tetrahedrally coordinated atoms (for example, Si), and imidazolate links replace oxygen bridges. Yaghi et al. highlight the similarities between ZIFs and zeolites by using the formulation $T(Im)_2$ (Im = imidazolate and its derivatives, T = tetrahedrally bonded metal ion or cluster) as an analog to $(Al)SiO_2$. In particular the T–Im–T angle of 145° is close to the Si–O–Si angle typically found in zeolites. The structure adopted by a ZIF is dependent on the link-link interactions present, as opposed to the structure directing agents used with zeolite synthesis.[67] Because of their exceptional thermal and chemical stability, ZIFs have held great promise as porous materials for a variety of applications.

In particular, Yaghi and co-workers reported the synthesis and characterization of two mesoporous ZIFs, ZIF-95 and ZIF-100, with structures of a scale and complexity previously unknown in zeolites (Figure 8).[47] ZIF-95 has a neutral framework with all Zn nodes tetrahedrally coordinated by cbIM (cbIM = 5-chlorobenzimidazole) with two types of cages. The pores of ZIF-95 are of ellipsoidal shape: from the van der Waals surfaces, the smaller cage measures $25.1 \times 14.3\,Å^2$, while the larger cage measures $30.1 \times 20.0\,Å^2$. ZIF-100 has a more complex structure with a 67.2 Å outer sphere diameter and a 35.6 Å inner sphere diameter. Thermal gravimetric analysis and powder X-ray diffraction studies revealed a thermal stability range up to 500°C for both ZIF-95 and ZIF-100. From N_2 and Ar adsorption isotherms, the Langmuir surface areas were $1{,}240\,m^2\,g^{-1}$ and $780\,m^2\,g^{-1}$ for ZIF-95 and ZIF-100, respectively.

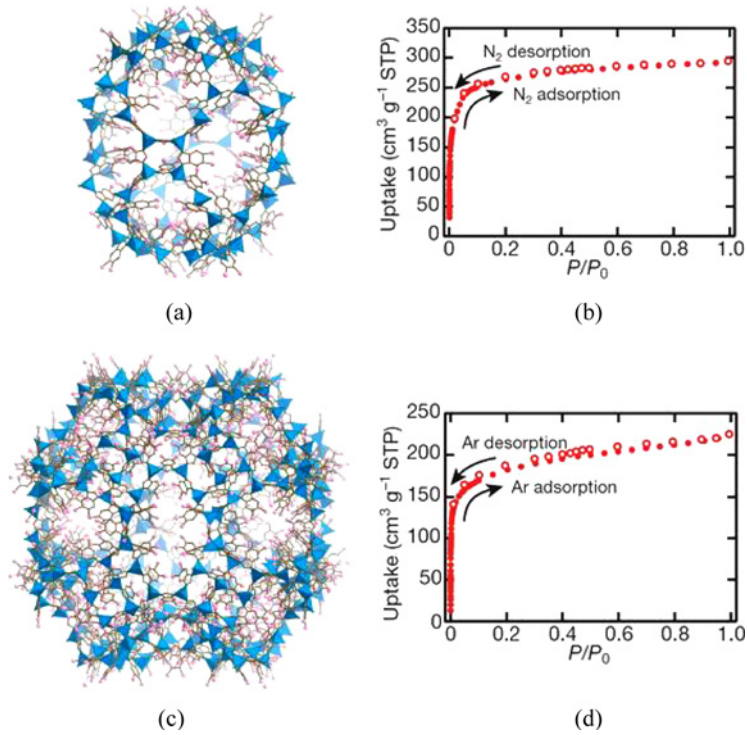

Figure 8. Structure of poz B cage with $30.1 \times 20.0\,\text{Å}^2$ (a) and N_2 sorption isotherm (b) in ZIF-95, and structure of moz cage with 35.6 Å inner sphere diameter (c) and N_2 sorption isotherm (d) of ZIF-100. (Reproduced with permission from Wang et al.[47] Copyright 2008: Nature Publishing Group.) (Figure appears in color online.)

3.5. Mesoporous MOFs Based on Supramolecular Templates

Differing from the traditional method to synthesize mesoporous MOFs, a novel supramolecular template strategy has been successfully applied to design mesostructured MOFs with tunable pore size, pore volume, and surface area.[48] Although supramolecular aggregates of surfactant molecules, such as micelles, have been widely used to develop various mesoporous molecular sieves and mesostructured metal oxides,[55,69,70] the application of such supramolecular templates to the design of mesostructured MOFs remains unexplored.

To illustrate the supramolecular template strategy for designing and preparing mesostructured MOFs with tailored porosity, Qiu et al. used the surfactant cetyltrimethylammonium bromide (CTAB) as a

structure-directing agent, and chose Cu^{2+} and the BTC ligand (BTC = benzene-1,3,5-tricarboxylate) as framework-building blocks.[48] A series of hierarchically porous MOFs with adjustable interconnecting micropores and mesopores was prepared by self-assembly of the framework-building blocks in the presence of surfactant micelles. The mesopore walls in these solids are formed from a crystalline microporous framework, HKUST-1,[27] containing a 3-D system of channels with a pore diameter of 0.82 nm, resulting in hierarchically micro- and mesoporous MOFs. The porosity properties of the mesostructured MOFs are tunable by varying the CTAB/Cu^{2+} molar ratio. The mesopore diameter of these mesostructured MOFs increases from 3.8 to 5.6 nm with increasing CTAB/Cu^{2+} molar ratio from 0.15 to 0.60. To obtain mesostructured MOFs with much larger mesopore sizes, a hydrophobic organic compound, 1,3,5-trimethylbenzene (TMB), was further chosen as an auxiliary structure-directing agent to swell the CTAB micelles. Remarkably, the mesopore diameter of the mesostructured MOF increases to 31.0 nm with the addition of TMB to the reaction mixture at a TMB/CTAB molar ratio of 0.50 when the CTAB/Cu^{2+} molar ratio is fixed at 0.30. All samples exhibit N_2 adsorption–desorption isotherms of a mode intermediate between Type I and Type IV with hysteresis loops, indicative of a 3-D intersecting network. The small-angle X-ray diffraction (SAXD) patterns of all the MOFs exhibit a single low-angle diffraction peak at a $2\theta = 1.3^\circ$, suggesting a disordered mesostructure without long-range order in the arrangement of the mesopores. Wide-angle X-ray diffraction (WAXD) patterns of the as-synthesized samples show the characteristic pattern of microporous HKUST-1. The results of TEM and selected-area electron diffraction further confirmed that the mesostructured MOFs consist of nanocrystalline domains of microporous HKUST-1. This work is the first example of the rational design of hierarchically porous MOFs with tunable porosity. An appropriate choice of supramolecular templates (for example, surfactants, block copolymers, and swelling agents) and a variation of the molar ratios of surfactant to framework-building blocks and of surfactant to swelling agent could be used to systematically control the porosity of such mesoporous MOFs.

4. APPLICATIONS OF MESOPOROUS MOFs

4.1. Gas Storage

A tank charged with a porous adsorbent enables an amount of gas to be stored at a much lower pressure than an identical tank without an

adsorbent. This provides a safer and more economical gas storage method since high-pressure tanks and multi-stage compressors can be avoided. Many gas storage studies have been conducted on porous adsorbents such as activated carbon, carbon nanotubes, and zeolites.[71,72] MOFs have received growing attention as such adsorbents due to their tunable pore geometries and flexible frameworks. A number of recent studies have been devoted to the adsorption of hydrogen, methane and carbon dioxide on such materials of which several have adsorption capacities that are equivalent or better than the current zeolite or activated carbon samples. Hydrogen is an attractive energy carrier because it is carbon-free and has an exceptional mass energy density.[73] The US Department of Energy (DOE) 2015 targets for a hydrogen storage system are: a capacity of 40 g H_2 per L, a refuelling time of 10 min or less, a lifetime of 1000 refuelling cycles, and an ability to operate within the temperature range -30 to 50°C.[74,75] In addition, carbon dioxide and methane are two of the principal greenhouse gases emitted today. The DOE has also set targets for carbon dioxide (56 wt%) and methane (18 wt%) storage systems.[76,77]

Recently, some mesoporous MOFs have been tested for their ability to store these gases (Table 2). For instance, the metal carboxylates, MIL-101, can adsorb large amounts of hydrogen at 77 K, with a capacity close to 6.1 wt% as well as the high heat of adsorption (10 kJ mol^{-1}) at low pressure.[78] Additionally, MIL-101 exhibits the highest carbon dioxide capacity with 40 mmol g^{-1} (303 K, 5 MPa). This leads to enormous volumes of carbon dioxide per volume of adsorbent, with a value of 390 v/v.[79] It should be noted that saturation occurs with large pore MOFs at much higher pressures than zeolites, which may be interesting for the recovery of CO_2 at high pressures from gas streams. In the case of methane, the uptake by MIL-101 is 13.6 mmol g-1 at 6 MPa, which is equivalent to the volume capacity within 135 $cm^3_{STP} \cdot cm^{-3}$ at 6 MPa.[79]

4.2. Gas Separation

Since the invention of synthetic zeolites in the 1940s, with the appearance of different adsorbents and the development of adsorption-based separation processes, adsorption has become an important gas separation tool in industry.[80–82] In addition, with the synthesis of more and more novel sorbent materials with tailor-made porosity and surface properties and the urgent demand for green separation procedures, adsorptive separation will become increasingly more significant. Thus,

Table 2. Comparison of gas storage of mesoporous MOFs

	H_2 storage				CO_2 storage				CH_4 storage				
			Conditions				Conditions				Conditions		
Compounds	Excess/ wt%	Vol./ g L^{-1}	P/bar	T/K	mmol g^{-1}	cm^3 cm^{-3}	P/bar	T/K	mmol g^{-1}	cm^3 cm^{-3}	P/bar	T/K	Ref.
MIL-100	0.15	1.04	73.3	298	18	280	50	304	9.5	150	60	303	[77],[78]
	3.28	23.0	90	77									
MIL-101	0.43	1.84	80	298	40	390	50	304	13.6	136	60	303	[77],[78]
	6.1	26.1	80	77									
UCMC-2	6.9		46	77									[46]
$Tb_{16}(TATB)_{16}(DMA)_{24}$					18		45	298					[45]

adsorptive separation may play a key role in future energy and environmental technologies.[83] In particular, it is now commonly believed that carbon dioxide emissions from the combustion of fossil fuels in power plants and automobiles are altering the global climate with undesirable consequences for the Earth's environment.[84] However, it is still a challenge to efficiently and selectively capture CO_2 from industrial emission streams (which invariably contain other gases such as CH_4, N_2 and so on).[85,86]

Interestingly, both mesoporous ZIFs prepared by the Yaghi laboratory, ZIF-95 and ZIF-100, can selectively capture carbon dioxide from several different gas mixtures at room temperature.[47] The two ZIFs thus uniquely combine huge cavities (24.0 Å and 35.6 Å for ZIF-95 and ZIF-100, respectively) and highly constricted windows (largest apertures, 3.65 Å and 3.35 Å, respectively), which points to their possible utility in carbon dioxide capture and storage. Both ZIFs show high affinity and capacity to reversibly adsorb/desorb CO_2 relative to methane, carbon monoxide and nitrogen based upon adsorption isotherms. ZIF-95 and ZIF-100 were shown to selectively adsorb CO_2 from mixtures of CO_2/CH_4, CO_2/CO or CO_2/N_2 (50:50 v/v). The results are shown in Figure 9 for CO_2/N_2 passing through 1.2 g ZIF-95 and CO_2/CH_4 passing through 1.1 g ZIF-100. These experiments showed that CO_2 was retained while the other gases passed through the pores.

4.3. Sensor

A commonly used dye, rhodamine 6 G (Rh6 G), is a xanthene derivative used as a gain medium in dye lasers, and it exhibits strong absorption in the visible region and a very high fluorescence quantum yield.[87,88] An increasing number of studies have recently tried to incorporate Rh6 G into hybrid organic–inorganic materials for applications in fields such as solid-state lasing, optical filters, and optoelectronics.[89–94]

Based on this issue, Qiu et al. assembled the mesoporous MOF, JUC-48, with Rh6 G dye molecules by adding Rh6 G in ethanol to the growth solution.[40] The amount of Rh6 G in the red-colored doped crystals was about 0.046% as determined by TG, ICP, and elemental analysis. The strongest emission peak of the fluorescence spectrum for JUC-48 · Rh6 G is at 563 nm with the excitation peak at 541 nm at room temperature, which is similar to the previous results obtained on Rh6 G-doped mesostructured materials.[95] Also, JUC-48 · Rh6 G can

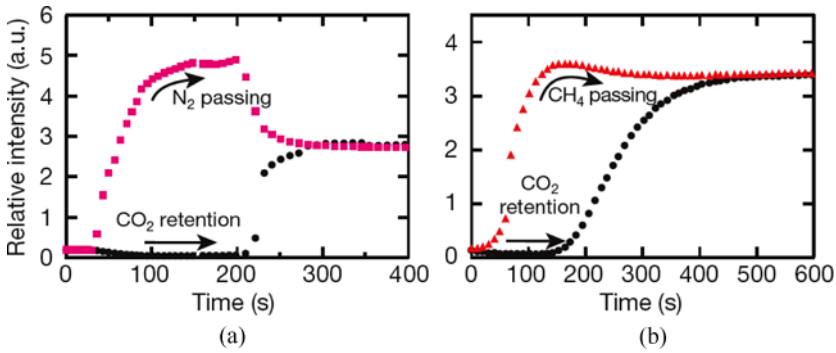

Figure 9. Breakthrough curves of ZIF-95 (a) for N_2 and CO_2 using a CO_2/N_2 gas mixture and ZIF-100 (b) for CH_4 and CO_2 using a CO_2/CH_4 gas mixture. (Reproduced with permission from Wang et al.[47] Copyright 2008: Nature Publishing Group.) (Figure appears in color online.)

be obtained by immersing JUC-48 in solutions of Rh6 G in ethanol with different concentrations. However, the emission peaks exhibit a blue shift when the concentration of the Rh6 G solution used to prepare JUC-48 · Rh6 G is decreased from 10^{-3} to 10^{-5} M, which implies that the Rh6 G dye in the crystals is present as free monomer molecules and shows fine fluorescence properties.[96] Of particular interest, JUC-48 · Rh6 G shows for the first time favorable temperature-dependent luminescent properties in a MOF. The peak location of JUC-48 · Rh6 G at 563 nm remains unchanged with decreasing temperature (from 298 K to 77 K), while the intensity of the signal is enhanced linearly, which reveals that JUC-48 · Rh6 G will be a potential candidate for applications in temperature-sensing devices.[97]

4.4. Catalysis

Development of practical catalysts for efficient synthesis is of key importance to the chemical industry.[98,99] Homogeneous catalysts have the advantages of high activity and selectivity, while heterogeneous catalysts are useful for their higher stability and ease of separation from the product.[99] In the past decade, utilizing MOFs as a new class of immobilized catalysts has been widely speculated. These materials, with proper functional groups, can be insoluble in the conventional reaction media and thus may potentially be useful in heterogeneous catalysis. Additionally, the activity of the framework may be modified by tailoring the linkers to adjust porosity or include chirality.[100]

The existence of coordinatively unsaturated metal sites (CUSs) is very useful. Chang and Férey et al. presented a new method for direct and selective coordination of electron-rich functional groups to chromium(III) CUSs in chromium(III) terephthalate MIL-101 with zeotypic giant pores and examined its catalytic consequences.[101] Trimeric chromium(III) octahedral clusters of MIL-101 possess terminal water molecules, removable from the framework after vacuum treatment at 423 K for 12 h, thus providing the CUS as Lewis acid sites in the structure usable for the surface functionalization.[102,103] The synthesis of the ethylenediamine (ED)-grafted MIL-101 (ED-MIL-101) by coordination of ED to the dehydrated MIL-101 framework was performed in toluene by heating to reflux. Diethylenetriamine (DETA) and 3-aminopropyltrialkoxysilane (APS) can also be used for the surface functionalization. ED-MIL-101 was determined by X-ray diffraction patterns, IR spectra and N_2 adsorption isotherms. The catalytic performance of dehydrated ED-MIL-101 in base catalysis was measured by using the Knoevenagel condensation as a base-catalyzed model reaction and its activities were compared to those of the APS-grafted mesoporous silica SBA-15 (APS-SBA-15).[104] For the condensation of benzaldehyde into *trans*-ethyl cyanocinnamate, the conversion for ED-MIL-101 is 97.1%, with high selectivity (99.1%). By contrast, APS-SBA-15 exhibits only 74.8% conversion, with 93.5% selectivity. Interestingly, ED-MIL-101 also reveals the size dependence on catalytic activities owing to the change of the substituent groups of carbonyl compounds in the Knoevenagel condensation. In additional studies, the encapsulation of noble metals, such as palladium, over the amine-grafted MIL-101 has been studied. Palladium-loaded APS-MIL-101 and ED-MIL-101 have obviously high activities during the Heck reaction at 393 K, and their activities were comparable with that of a commercial Pd/C catalyst (1.09 wt% Pd) after a certain induction period (0.5–1 h), probably owing to the slow diffusion of reactants to reach accessible metal sites in the pores.

4.5. Drug Delivery

Currently, considerable attention has been devoted to the development of methods to control drug release to satisfy the ever-growing demand for prolonged and better control of drug administration. Up to now, two routes have been used. In the "organic route" biocompatible dendrimers or polymers are used to introduce drugs into a system.[105,106] In this case,

a wide range of drugs can be encapsulated but a controlled release is difficult to achieve in the absence of well-defined porosity. The other method is the "inorganic route" in which the hosts are inorganic porous solids, such as zeolites[107,108] or mesoporous silicate materials.[109] The release of inorganic porous solids is performed by grafting organic molecules on the pore walls but implies a decrease in the drug-loading capacity.[110,111] However, mesoporous MOFs could present a third way: the "hybrid" route based upon both regular porosity and organic functionality.

Férey et al. have explored the adsorption and delivery of a model analgesic and anti-inflammatory drug, ibuprofen (IBU), by MIL-100 and MIL-101.[112] IBU was adsorbed by the dehydrated powdered materials from a solution in hexane, and the amount adsorbed was determined by TG analysis, UV/Vis spectroscopy and elemental analysis; the presence of IBU was also confirmed by IR spectroscopy. Additionally, solid-state ^{1}H and ^{13}C NMR experiments were performed on IBU and the anhydrous MIL-100/IBU and MIL-101/IBU. The MIL-100 and MIL-101 materials showed remarkable IBU adsorption. The MIL-100 matrix has smaller cages (25 and 29 Å) and adsorbs 0.35 g of IBU/gram of dehydrated MIL-100. MIL-101 with its larger cage sizes (29 and 34 Å; pore volumes: 12 700 and 20 600 $Å^3$) shows an unprecedented amount of adsorbed drug, larger than the initial matrix weight ($\approx$ 1.4 grams of IBU/gram of dehydrated MIL-101). On the other hand, MIL-101 and MIL-100 were compacted as cylindrical pieces to study the kinetics of IBU delivery. It is noted that the performances of these two mesoporous MOFs for drug delivery can be compared to those of similar materials with comparable cage sizes, such as MCM-41 with a pore diameter of 36 Å.[110] MCM-41 and MIL-100 materials showed very similar IBU dosage and kinetics. However, the drug content of MIL-101 is four times larger than in MCM-41 and the delivery time is longer, taking six days for MIL-101 compared to two days for MCM-41 for full release. MIL-101 thus would allow a higher dosage of drug and a longer controlled delivery, which supports the proposed advantages of mesoporous MOFs for larger pharmacological molecules.

5. CONCLUDING REMARKS

MOFs as a new member of porous materials have recently become a topic of central importance to inorganic and materials chemistry. Many studies on MOFs are flourishing with exciting new findings in the areas

of gas storage, sensing, separation, optics, nanoreactors and catalysis. Although MOFs have greatly expanded the scope of porous materials, they are largely restricted to the microporous domain. In order to study the potential applications of these materials in a wider range of fields, several mesoporous MOFs with channels or cavities over 2 nm have been synthesized. Based on the potential advantages offered by mesoporous MOFs, it is anticipated that the number of such mesoporous materials, particularly those involving functional organic linkers, will grow substantially in the near future. Additionally, the surface functionalization of mesoporous MOFs should allow for stabilization of these materials and the possibility of conjugation to biomolecules for use in biomedical and biotechnology applications. It is believed that mesoporous MOFs will provide extraordinary advantages over microporous MOF materials, which we anticipate will have an important and permanent impact on the future of porous compounds.

REFERENCES

1. Breck, D. W. 1974. *Zeolite Molecular Sieves: Structure, Chemistry, and Use*, Wiley, New York.
2. Meier, W. M., D. H. Olsen, and C. Baerlocher. 1996. *Atlas of Zeolite Structure Types*, Elsevier, London.
3. Venuto, P. B. 1994. *Microporous Mater.*, **2** (5): 297–411.
4. Kresge, C. T., M. E. Leonowicz, W. J. Roth, J. C. Vartuli, and J. S. Beck. 1992. *Nature*, **359** (6397): 710–712.
5. Roberts, P. V., D. M. Mackay, and F. S. Cannon. 1980. Preparation and Evaluation of Powdered Activated Carbon from Lignocellulosic Materials, Environmental Protection Agency, Office of Research and Development, Municipal Environmental Research Laboratory, Springfield, VA.
6. Sing, K. S. W. 1985. *Pure Appl. Chem.*, **57** (4): 603–619.
7. Brunauer, S., L. S. Deming, W. E. Deming, and E. Teller. 1940. *J. Am. Chem. Soc.*, **62** (7): 1723–1732.
8. Gregg, S. J. and K. S. W. Sing. 1984. *Adsorption, Surface Area, and Porosity*, Academic Press, London.
9. Bailar, J. C. 1964. *Prep. Inorg. React.*, **1**: 1–27.
10. Chen, C.-T. and K. S. Suslick. 1993. *Coord. Chem. Rev.*, **128** (1–2): 293–322.
11. Yaghi, O. M., H. L. Li, C. Davis, D. Richardson, and T. L. Groy. 1998. *Acc. Chem. Res.*, **31** (8): 474–484.
12. Kitagawa, S. and M. Kondo. 1998. *Bull. Chem. Soc. Jpn.*, **71**: 1739–1753.
13. Robson, R. 2000. *J. Chem. Soc., Dalton Trans.*, (21): 3735–3744.

14. Eddaoudi, M., D. B. Moler, H. L. Li, B. L. Chen, T. M. Reineke, M. O'Keeffe, and O. M. Yaghi. 2001. *Acc. Chem. Res.*, **34** (4): 319–330.
15. Moulton, B. and M. J. Zaworotko. 2001. *Chem. Rev.*, **101** (6): 1629–1658.
16. Yaghi, O. M., M. O'Keeffe, N. W. Ockwig, H. K. Chae, M. Eddaoudi, and J. Kim. 2003. *Nature*, **423** (6941): 705–714.
17. James, S. L. 2003. *Chem. Soc. Rev.*, **32** (5): 276–288.
18. Janiak, C. 2003. *J. Chem. Soc., Dalton Trans.*, (14): 2781–2804.
19. Kitagawa, S., R. Kitaura, and S. I. Noro. 2004. *Angew. Chem. Int. Ed.*, **43** (18): 2334–2375.
20. Rao, C. N. R., S. Natarajan, and R. Vaidhyanathan. 2004. *Angew. Chem. Int. Ed.*, **43** (12): 1466–1496.
21. Ferey, G., C. Mellot-Draznieks, C. Serre, and F. Millange. 2005. *Acc. Chem. Res.*, **38** (4): 217–225.
22. Maspoch, D., D. Ruiz-Molina, and J. Veciana. 2004. *J. Mater. Chem.*, **14** (18): 2713–2723.
23. Kitagawa, S. and K. Uemura. 2005. *Chem. Soc. Rev.*, **34** (2): 109–119.
24. Kitagawa, S., S. Noro, and T. Nakamura. 2006. *Chem. Commun.*, **42** (7): 701–707.
25. Mueller, U., M. Schubert, F. Teich, H. Puetter, K. Schierle-Arndt, and J. Pastre. 2006. *J. Mater. Chem.*, **16** (7): 626–636.
26. Ferey, G. 2008. *Chem. Soc. Rev.*, **37** (1): 191–214.
27. Chui, S. S. Y., S. M. F. Lo, J. P. H. Charmant, A. G. Orpen, and I. D. Williams. 1999. *Science*, **283** (5405): 1148–1150.
28. O'Keeffe, M., M. Eddaoudi, H. L. Li, T. Reineke, and O. M. Yaghi. 2000. *J. Solid State Chem.*, **152** (1): 3–20.
29. O'Keeffe, M. and B. G. Hyde. 1996. *Crystal Structures I: Patters and Symmetry.* Mineralogical Society of America, Washington, DC, 1996.
30. Batten, S. R. and R. Robson. 1998. *Angew. Chem. Int. Ed.*, **37** (11): 1460–1494.
31. Cheetham, A. K., G. Ferey, and T. Loiseau. 1999. *Angew. Chem. Int. Ed.*, **38** (22): 3268–3292.
32. Rosseinsky, M. J. 2004. *Microporous Mesoporous Mater.*, **73** (1–2): 15–30.
33. Rowsell, J. L. C. and O. M. Yaghi. 2004. *Microporous Mesoporous Mater.*, **73** (1–2): 3–14.
34. Wang, Z. and S. M. Cohen. 2009. *Chem. Soc. Rev.*, **38** (5): 1315–1329.
35. Murray, L. J., M. Dinca, and J. R. Long. 2009. *Chem. Soc. Rev.*, **38** (5): 1294–1314.
36. Ma, L., C. Abney, and W. Lin. 2009. *Chem. Soc. Rev.*, **38** (5): 1248–1256.
37. Li, J.-R., R. J. Kuppler, and H.-C. Zhou. 2009. *Chem. Soc. Rev.*, **38** (5): 1477–1504.
38. Eddaoudi, M., J. Kim, N. Rosi, D. Vodak, J. Wachter, M. O'Keeffe, and O. M. Yaghi. 2002. *Science*, **295** (5554): 469–472.

39. Wang, X. S., S. Q. Ma, D. F. Sun, S. Parkin, and H. C. Zhou. 2006. *J. Am. Chem. Soc.*, **128** (51): 16474–16475.
40. Fang, Q. R., G. S. Zhu, Z. Jin, Y. Y. Ji, J. W. Ye, M. Xue, H. Yang, Y. Wang, and S. L. Qiu. 2007. *Angew. Chem. Int. Ed.*, **46** (35): 6638–6642.
41. Koh, K., A. G. Wong-Foy, and A. J. Matzger. 2008. *Angew. Chem. Int. Ed.*, **47** (4): 677–680.
42. Ferey, G., C. Serre, C. Mellot-Draznieks, F. Millange, S. Surblé, J. Dutour, and I. Margiolaki. 2004. *Angew. Chem. Int. Ed.*, **43** (46): 6296–6301.
43. Ferey, G., C. Mellot-Draznieks, C. Serre, F. Millange, J. Dutour, S. Surble, and I. Margiolaki. 2005. *Science*, **309** (5743): 2040–2042.
44. Sonnauer, A., F. Hoffmann, M. Froba, L. Kienle, V. Duppel, M. Thommes, C. Serre, G. Ferey, and N. Stock. 2009. *Angew. Chem. Int. Ed.*, **48** (21): 3791–3794.
45. Park, Y. K., S. B. Choi, H. Kim, K. Kim, B. H. Won, K. Choi, J. S. Choi, W. S. Ahn, N. Won, S. Kim, D. H. Jung, S. H. Choi, G. H. Kim, S. S. Cha, Y. H. Jhon, J. K. Yang, and J. Kim. 2007. *Angew. Chem. Int. Ed.*, **46** (43): 8230–8233.
46. Koh, K., A. G. Wong-Foy, and A. J. Matzger. 2009. *J. Am. Chem. Soc.*, **131** (12): 4184–4185.
47. Wang, B., A. P. Cote, H. Furukawa, M. O'Keeffe, and O. M. Yaghi. 2008. *Nature*, **453** (7192): 207–211.
48. Qiu, L.-G., T. Xu, Z.-Q. Li, W. Wang, Y. Wu, X. Jiang, X.-Y. Tian, and L.-D. Zhang. 2008. *Angew. Chem. Int. Ed.*, **47** (49): 9487–9491.
49. Zhao, D., D. Yuan, D. Sun, and H.-C. Zhou. 2009. *J. Am. Chem. Soc.*, **131** (26): 9186–9188.
50. Beck, J. S., J. C. Vartuli, W. J. Roth, M. E. Leonowicz, C. T. Kresge, K. D. Schmitt, C. T. W. Chu, D. H. Olson, and E. W. Sheppard. 1992. *J. Am. Chem. Soc.*, **114** (27): 10834–10843.
51. Sayari, A. 1996. *Chem. Mater.*, **8** (8): 1840–1852.
52. Kruk, M., M. Jaroniec, and A. Sayari. 1997. *Langmuir*, **13** (23): 6267–6273.
53. Oye, G., W. R. Glomm, T. Vralstad, S. Volden, H. Magnusson, M. Stocker, and J. Sjoblom. 2006. *Adv. Colloid Interface Sci.*, **123**: 17–32.
54. Vartuli, J. C. and T. F. Degnan. 2007. *Stud. Surf. Sci. Catal.*, **168**: 837–854.
55. Davis, M. E. 2002. *Nature*, **417** (6891): 813–821.
56. Inagaki, S. 2004. *Stud. Surf. Sci. Catal.*, **148**: 109–116.
57. Mori, T., T. Yanagisawa, and N. Taira. 1990. *Jpn. J. Pharmacol.*, **52** (2): 263–271.
58. Zhao, D., Q. Huo, J. Feng, B. F. Chmelka, and G. D. Stucky. 1998. *J. Am. Chem. Soc.*, **120** (24): 6024–6036.
59. Tanev, P. T., M. Chibwe, and T. J. Pinnavaia. 1994. *Nature*, **368** (6469): 321–323.

60. Vartuli, J. C., W. J. Roth, and T. F. Degnan. 2004. *Dekker Encyclopedia of Nanoscience and Nanotechnology*, 1791.
61. Diaz, I., C. Marquez-Alvarez, F. Mohino, J. Perez-Pariente, and E. Sastre. 2000. *J. Catal.*, **193** (2): 283–294.
62. Diaz, I., C. Marquez-Alvarez, F. Mohino, J. Perez-Pariente, and E. Sastre. 2000. *J. Catal.*, **193** (2): 295–302.
63. Bennett, M. J. and J. V. Smith. 1968. *Mater. Res. Bull*, 3.
64. Park, K. S., Z. Ni, A. P. Cote, J. Y. Choi, R. Huang, F. J. Uribe-Romo, H. K. Chae, M. O'Keeffe, and O. M. Yaghi. 2006. *PNAS*, **103** (27): 10186–10191.
65. Huang, X.-C., Y.-Y. Lin, J.-P. Zhang, and X.-M. Chen. 2006. *Angew. Chem. Int. Ed.*, **45** (10): 1557–1559.
66. Tian, Y. Q., Y. M. Zhao, Z. X. Chen, G. N. Zhang, L. H. Weng, and D. Y. Zhao. 2007. *Chem.-Eur. J.*, **13** (15): 4146–4154.
67. Hayashi, H., A. P. Cote, H. Furukawa, M. O'Keeffe, and O. M. Yaghi. 2007. *Nat. Mater.*, **6** (7): 501–506.
68. Banerjee, R., A. Phan, B. Wang, C. Knobler, H. Furukawa, M. O'Keeffe, and O. M. Yaghi. 2008. *Science*, **319** (5865): 939–943.
69. Hartmann, S., D. Brandhuber, and N. Husing. 2007. *Acc. Chem. Res.*, **40** (9): 885–894.
70. Yang, P., D. Zhao, D. I. Margolese, B. F. Chmelka, and G. D. Stucky. 1998. *Nature*, **396** (6707): 152–155.
71. Morris, R. E. and P. S. Wheatley. 2008. *Angew. Chem. Int. Ed.*, **47** (27): 4966–4981.
72. Xiang, Z., J. Lan, D. Cao, X. Shao, W. Wang, and D. P. Broom. 2009. *J. Chem. Phys. C*, **113** (34): 15106–15109.
73. Berg, A. W. C. v. d. and C. O. Arean. 2008. *Chem. Commun.*, **6**: 668–681.
74. DoE Office of Energy Efficiency and Renewable Energy Hydrogen F. C. I. T. P. 2006. "Grand Challenge" for Basic and Applied Research in Hydrogen Storage Solicitation, last modified April 14, 2006, http://www.eere.energy.gov/hydrogenandfuelcells/2003_storage_solicitation.html
75. DoE Office of Energy Efficiency and Renewable Energy Hydrogen, Fuel Cell Technologies Program, Multi-Year Research, Development and Demonstration Plan: Planned Program Activities for 2005–2015, last modified October 1, 2009, http://www.eere.energy.gov/hydrogenandfuelcells/mypp
76. Kikkinides, E. S., R. T. Yang, and S. H. Cho. 1993. *Ind. Eng. Chem. Res.*, **32** (11): 2714–2720.
77. Kikuchi, R. 2003. *Energy Environ.*, **14**: 383–395.
78. Latroche, M., S. Surblé, C. Serre, C. Mellot-Draznieks, P. L. Llewellyn, J.-H. Lee, J.-S. Chang, S. H. Jhung, and G. Férey. 2006. *Angew. Chem. Int. Ed.*, **45** (48): 8227–8231.

79. Llewellyn, P. L., S. Bourrelly, C. Serre, A. Vimont, M. Daturi, L. Hamon, G. De Weireld, J.-S. Chang, D.-Y. Hong, Y. Kyu Hwang, S. Hwa Jhung, and G. Ferey. 2008. *Langmuir*, **24** (14): 7245–7250.
80. Xu, R., W. Pang, J. Yu, Q. Huo, and J. Chen. 2007. *Chemistry of Zeolites and Related Porous Materials: Synthesis and Structure*, John Wiley & Sons (Asia), Singapore, p. 679.
81. Yang, R. T. 1997. *Gas Separation by Adsorption Processes*, World Scientific, London, Vol. 1.
82. Rouquerol, F., I. Rouquerol, and K. Sing. 1999. *Adsorption by Powders and Porous Solids-Principles Methodology and Applications*, Academic Press, London.
83. Yang, R. T. 2003. *Adsorbents: Fundamentals and Applications*, Wiley-Interscience, Hoboken, NJ.
84. Wigley, T. M. L., A. K. Jain, F. Joos, B. S. Nyenzi, and P. R. Shukla. 1997. *Implications of Proposed CO_2 Emissions Limitations*, Intergovernmental Panel on Climate Change, Geneva, Switzerland.
85. Sircar, S. 2006. *Ind. Eng. Chem. Res.*, **45**: 5435–5448.
86. Sasaki, A., S. Matsumoto, M. Fujitsuka, T. Shinoki, and T. Tanaka. 1993. *IEEE Trans. Energy Convers.*, **8**: 26–32.
87. Brackmann, U. 2000. *Laser Dyes*, Lambda Physik AG, Göttingen.
88. Valeur, B. 2002. *Molecular Fluorescence: Principles and Applications*, Weinheim, New York.
89. Yang, P., G. Wirnsberger, H. C. Huang, S. R. Cordero, M. D. McGehee, B. Scott, T. Deng, G. M. Whitesides, B. F. Chmelka, S. K. Buratto, and G. D. Stucky. 2000. *Science*, **287** (5452): 465–467.
90. Vogel, R., P. Meredith, I. Kartini, M. Harvey, J. D. Riches, A. Bishop, N. Heckenberg, M. Trau, and H. Rubinsztein-Dunlop. 2003. *Chemphyschem*, **4** (6): 595–603.
91. Kalogeras, I. M., E. R. Neagu, and A. Vassilikou-Dova. 2004. *Macromolecules*, **37** (3): 1042–1053.
92. Loerke, J. and F. Marlow. 2002. *Adv. Mater.*, **14** (23): 1745–1749.
93. Wirnsberger, G., P. Yang, H. C. Huang, B. Scott, T. Deng, G. M. Whitesides, B. F. Chmelka, and G. D. Stucky. 2001. *J. Phys. Chem. B.*, **105** (27): 6307–6313.
94. del Monte, F., J. D. Mackenzie, and D. Levy. 2000. *Langmuir*, **16** (19): 7377–7382.
95. Marlow, F., M. D. McGehee, D. Y. Zhao, B. F. Chmelka, and G. D. Stucky. 1999. *Adv. Mater.*, **11** (8): 632–636.
96. Barranco, A. and P. Groening. 2006. *Langmuir*, **22** (16): 6719–6722.
97. Sun, Y., K. Ye, H. Zhang, J. Zhang, L. Zhao, B. Li, G. Yang, B. Yang, Y. Wang, S. W. Lai, and C. M. Che. 2006. *Angew. Chem. Int. Ed.*, **45** (34): 5610–5613.

98. Cornils, B., W. A. Herrmann, M. Muhler, and C.-H. Wong. 2007. *Catalysis from A to Z : A Concise Encyclopedia*, Wiley-VCH, Weinheim, Vol. 3.
99. Sheldon, R. A., I. Arends, and U. Hanefeld. 2007. *Green Chemistry and Catalysis*, Wiley-VCH, Weinheim.
100. Wang, Z., G. Chen, and K. Ding. 2009. *Chem. Rev.*, **109** (2): 322–359.
101. Hwang, Y. K., D. Y. Hong, J. S. Chang, S. H. Jhung, Y. K. Seo, J. Kim, A. Vimont, M. Daturi, C. Serre, and G. Ferey. 2008. *Angew. Chem. Int. Ed.*, **47** (22): 4144–4148.
102. Li, H., C. E. Davis, T. L. Groy, D. G. Kelley, and O. M. Yaghi. 1998. *J. Am. Chem. Soc.*, **120** (9): 2186–2187.
103. Vimont, A., H. Leclerc, F. Mauge, M. Daturi, J.-C. Lavalley, S. Surble, C. Serre, and G. Ferey. 2007. *J. Phys. Chem. C.*, **111** (1): 383–388.
104. Wang, X. G., Y. H. Tseng, J. C. C. Chan, and S. F. Cheng. 2005. *J. Catal.*, **233** (2): 266–275.
105. Freiberg, S. and X. Zhu. 2004. *Int. J. Pharm.*, **282** (1–2): 1–18.
106. Soppimath, K. S., T. M. Aminabhavi, A. R. Kulkarni, and W. E. Rudzinski. 2001. *J. Controlled Release*, **70** (1–2): 1–20.
107. Shivanand, P. and O. L. Sprockel. 1998. *Int. J. Pharm.*, **167** (1–2): 83–96.
108. Rivera, A. and T. Farias. 2005. *Microporous Mesoporous Mater.*, **80** (1–3): 337–346.
109. Vallet-Regi, M., A. Ramila, R. P. del Real, and J. Perez-Pariente. 2001. *Chem. Mater.*, **13** (2): 308–311.
110. Munoz, B., A. Ramila, J. Perez-Pariente, I. Diaz, and M. Vallet-Regi. 2003. *Chem. Mater.*, **15** (2): 500–503.
111. Horcajada, P., A. Ramila, F. Gerard, and M. Vallet-Regi. 2006. *Solid State Sci.*, **8** (10): 1243–1249.
112. Horcajada, P., C. Serre, M. Vallet-Regi, M. Sebban, F. Taulelle, and G. Ferey. 2006. *Angew. Chem. Int. Ed.*, **45** (36): 5974–5978.